Inorganic Chemistry

Article

pubs.acs.org/IC

Crystal Structure and a Giant Magnetoresistance Effect in the New Zintl Compound $Eu_3Ga_2P_4$

Naohito Tsujii,*[,†,‡] Catherine A. Uvarov,[‡] Peter Klavins,[§] Tanghong Yi,[‡] and Susan M. Kauzlarich[‡]

[†]National Institute for Materials Science, Sengen 1-2-1, Tsukuba 305-0047, Japan

[‡]Department of Chemistry and [§]Department of Physics, University of California, Davis, One Shields Avenue, Davis, California 95616, United States

Supporting Information

ABSTRACT: Single-crystalline samples of a new Zintl compound, $Eu_3Ga_2P_4$, have been synthesized by a Ga-flux method. $Eu_3Ga_2P_4$ is found to crystallize in a monoclinic unit cell, space group $C2/c$, isostructural to $Ca_3Al_2As_4$. The structure is composed of a pair of edge-shared GaP_4 tetrahedra, which link by corner-sharing to form Ga_2P_4 two-dimensional layers, separated by Eu^{2+} ions. Magnetic susceptibility showed a Curie–Weiss behavior with an effective magnetic moment consistent with the value for Eu^{2+} magnetic ions. Below 15 K, ferromagnetic ordering was observed and the saturation magnetic moment was 6.6 μ_B. Electrical resistivity measurements on a single crystal showed semiconducting behavior. Resistivity in the temperature range between 280 and 300 K was fit by an activation model with an energy gap of 0.552(2) eV. The temperature dependence of the resistivity is better described by the variable-range-hopping model for a three-dimensional conductivity, suggesting that Eu–P bonds are involved in the conductivity. A large magnetoresistance, up to −30%, is observed with a magnetic field H = 2 T at T = 100 K, suggesting strong coupling of carriers with the Eu^{2+} magnetic moment.

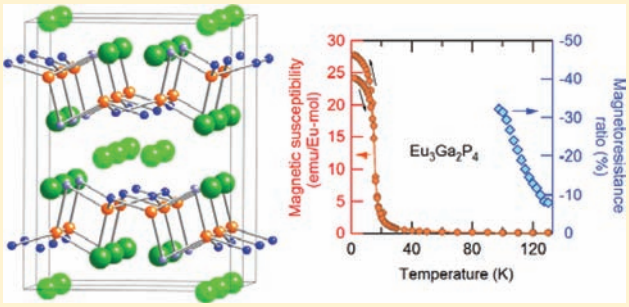

INTRODUCTION

Zintl phases are valence-precise compounds built up of electropositive elements including alkaline, alkaline-earth, and rare-earth atoms, with electronegative main-group elements.[1] Zintl compounds with Eu or Yb are particularly interesting because they can show multiple valence states, either divalent or trivalent, with different magnetic states, which adds to the Zintl phases more diversity in the structure and useful physical properties for functional materials.[2,3]

In fact, the Zintl compound $Eu_{14}MnSb_{11}$ shows a ferromagnetic transition with a colossal magnetoresistance (CMR).[4] CMR is the dramatic change (greater than 5–10%) in resistance as a function of the magnetic field and occurs at the magnetic ordering temperature. This is primarily observed in manganese-based oxides[5,6] and is unusual for Zintl compounds. In this compound, both the Eu^{2+} and Mn^{3+} ions have magnetic moments, whereas the magnetic moment of Mn^{3+} is responsible for the CMR observed around T_C.[4] The isostructural compound $Yb_{14}MnSb_{11}$ shows peculiar thermoelectric properties with dimensionless figure of merit $zT \sim 1$.[7] In $Yb_{14}MnSb_{11}$, Yb ions are divalent,[8] thereby nonmagnetic and similar to alkaline-earth elements. In these examples, the Mn ions appear to play a more important role in the physical properties rather than the rare-earth elements.

On the other hand, our preceding research identified several Zintl compounds where only Eu ions carry magnetic moments.[9−13] $EuIn_2P_2$ and $EuGa_2P_2$ show CMR over −300% and −80%, respectively.[11,13] The behavior is due to Eu^{2+} ions, indicating that Eu ions are not simply donating electrons but also have strong interaction with carriers. Both of the two compounds show metallic behavior around room temperature. Below about 60 K, the resistivity turns into semiconducting behavior with a very narrow energy gap, which collapses by a few tesla of the magnetic field.[11,13] A strong coupling of magnetism and carriers is also suggested by the magnetooptical measurement.[14] Among compounds with a rare earth as the only magnetic element, such a large magnetoresistance (MR) has only been observed for limited cases such as EuB_6[15,16] and EuO or Eu-containing monocalchogenides.[17−19] These examples point to the importance of the investigation of rare earths containing Zintl phases because they can bring new strategies to finding useful functional materials.

It is noted that the two Zintl compounds, $EuIn_2P_2$ and $EuGa_2P_2$, have new crystal structure types.[11−13,20] $EuIn_2P_2$ has a hexagonal unit cell with the space group $P6_3/mmc$. $EuGa_2P_2$ has a monoclinic unit cell with space group $P2/m$. In both compounds, ethane-like $P_3M–MP_3$ moieties exist with M = In or Ga, which are connected by corner-sharing sequences to form a layer. The In–In distance within the $P_3In–InP_3$ moiety for $EuIn_2P_2$ is 2.7608 Å, which is shorter than twice that of the In covalent radius, 3.0 Å. For $EuGa_2P_2$, the Ga–Ga distances

Received: September 14, 2011
Published: February 16, 2012

   dx.doi.org/10.1021/ic202018r | Inorg. Chem. 2012, 51, 2860–2866

range from 2.4048 to 2.4922 Å, again slightly shorter than twice that of the Ga covalent radius, 2.5 Å. These facts suggest the existence of unusual M−M covalent bonding. In fact, charge compensation seems to be incomplete in these two compounds because they show metallic conductivity. This is similar to the Zintl phase compounds $Ba_2In_2Pn_5$ (Pn = P and As), which have direct In−In bonds and show metallic conductivity.[21] Notably, the single-crystalline X-ray diffraction for $EuGa_2P_2$ has suggested the presence of a minor phase in the crystal, in which the structure is derived by a partial substitution of Eu for some Ga−Ga dumbbells. As a result, the minor phase may have a chemical composition $Eu_3Ga_2P_4$.[13] The suggested structure for $Eu_3Ga_2P_4$ has a one-dimensional chain composed of P_3Ga−GaP_3 units. Similar structural relationship from 1−2−2 type to 3−2−4 type compounds has been discussed for $BaGa_2As_2$.[22] Out of the Ga_2As_2 layer in $BaGa_2As_2$, three different types of one-dimensional chain structures are derived, namely, the $Ca_3Si_2As_4$, $Ba_3Sn_2P_4$, and $Sr_3Si_2As_4$ types. In addition, $Eu_3Ga_2P_4$ can be a charge-balanced new Zintl phase if the formal valence of $Eu_3Ga_2P_4$ is expressed as $(Eu^{2+})_3(Ga^{3+})_2(P^{3-})_4$. A Zintl compound with a similar chemical composition, $Eu_3In_2P_4$, is indeed reported to exist and is shown to be a semiconductor with an energy gap of 0.42−0.45 eV.[10,23] One can therefore expect the existence of a new magnetic Zintl compound, $Eu_3Ga_2P_4$, as well.

We, hence, tried to synthesize $Eu_3Ga_2P_4$ and have successfully grown its single crystals using a Ga-flux technique. The structure was determined to be isostructural to $Ca_3Al_2As_4$,[24] quite different from the expected $EuGa_2P_2$-derived structure or the $Sr_3In_2P_4$-type structure in which $Eu_3In_2P_4$ crystallizes.[25] Electrical resistivity of $Eu_3Ga_2P_4$ showed a semiconducting behavior, consistent with the Zintl concept. Magnetic measurements revealed ferromagnetic behavior below 15 K with a saturation moment of 6.6 μ_B per Eu. A large negative MR, −30%, is observed at 100 K for an applied field of 2 T.

EXPERIMENTAL SECTION

Synthesis. Single crystals of $Eu_3Ga_2P_4$ were synthesized by a molten Ga-flux reaction. Typical flux growth procedures are reported in the literature.[26,27] Pure elements of Eu (Ames Laboratory, 99.999%), Ga (Furuchi Chem., 99.999%), and P (Johnson Matthey, 99.9999%) were loaded in an alumina crucible with the atomic ratio Eu:Ga:P = 3:120:4. The crucible was placed in a quartz tube, over which quartz wool of about 5 cm^3 was placed. These steps were carried out in a nitrogen-filled drybox with a water concentration of less than 1 ppm. The quartz tube was evacuated and sealed under vacuum. Then the sealed tube was heated up to 770 K in 2 h, kept at 770 K for 2 h, ramped again to 1370 K in 2 h, kept at 1370 K for 16 h, and then cooled slowly at a rate of −3 K/h to 1120 K, at which time the tube was quickly removed from the oven, inverted, and centrifuged. The tube was then opened in the drybox. Dark-gray needle-shaped crystals were collected from of the crucible. The compound was found to be sensitive to air and water. When exposed to ambient atmosphere, the compound decomposes into a gray-yellowish powder within 1 h. All of the samples were stored in the drybox.

Single-Crystal X-ray diffraction. The crystal structure of $Eu_3Ga_2P_4$ was identified by single-crystal X-ray diffraction. Diffraction data were collected using a Bruker Smart Apex II diffractometer at 90 K. A single crystal was cut into a small piece with a size of 0.06 × 0.05 × 0.02 mm^3. The crystal was handled with Paratone-N oil on the surface to avoid decomposition. It was mounted on a quartz fiber and cooled by a cold N_2 stream. The diffraction data were obtained with graphite-monochromated Mo Kα radiation. An absorption correction was applied using the *SADABS 2.1* program.[28] The structure solution was obtained by direct methods using the Bruker *SHELXTL* program.[29]

Magnetization Measurements. Magnetic property measurements were carried out using a Quantum Design MPMS superconducting quantum interference device (SQUID) magnetometer. A small single crystal, with a mass of 2.74 mg, was used. The magnetic susceptibility was measured at a constant field of H = 100 G from 2 to 300 K. The field dependence of magnetization was measured at 2 K up to 5 T.

Electrical Resistivity Measurements. Electrical resistivity was measured using a four-probe method for a single-crystal sample. Platinum leads were attached on a cleaved crystal surface using silver paint. The cross-sectional area of the sample was approximately 0.23 mm^2, and the length between the electrical contacts was approximately 0.28 mm. The current was applied parallel to the b axis. This method was only applicable down to 200 K because of the high resistance of the sample. To obtain data at lower temperatures, the sample was cut into a smaller piece, and a two-probe method was employed. With this setup, resistance was measured down to 98 K, although the absolute values of the resistivity are not available. The sample was loaded into the SQUID chamber, with which temperature control and application of a magnetic field were carried out.

RESULTS AND DISCUSSION

Structural Characterization. Single-crystal X-ray diffraction revealed that $Eu_3Ga_2P_4$ has a monoclinic unit cell, space group $C2/c$, with lattice dimensions a = 13.0245(12) Å, b = 10.1167(10) Å, c = 6.5580(6) Å, and β = 90.2430(10)°. Selected data of crystallography and refinement conditions are listed in Table 1.

Table 1. Selected Crystallographic Data and Refinement Conditions for $Eu_3Ga_2P_4$

fw, g/mol	719.20
temperature, K	90(2)
wavelength, Å	0.710 73
cryst syst	monoclinic
space group	$C2/c$
unit cell dimens	a = 13.0245(12) Å
	b = 10.1167(10) Å
	c = 6.5580(6) Å
	β = 90.2430(10)°
volume, $Å^3$	864.11(14)
Z	4
density (calcd), g/cm^3	5.5286
abs coeff	28.256
final R indices $[I > 2\sigma(I)]^a$	R1 = 0.0214, wR2 = 0.0531
R indices (all data)	R1 = 0.0245, wR2 = 0.0545

^{a}R1 = $[\sum||F_o| - |F_c||]/\sum|F_o|$; wR2 = $\{[\sum w[(F_o)^2 - (F_c)^2]^2]\}^{1/2}$; w^{-1} = $[\sigma^2(F_o) + (0.0471P)^2 + (0.5945P)]$, where P = $[\max(F_o^2,0) + 2F_c^2/3]$.

The determined crystal structure is depicted in Figure 1. The compound is isostructural to $Ca_3Al_2As_4$.[24] Compounds with this structure type include $Ba_3In_2P_4$,[30] $Sr_3Al_2P_4$,[31] and $Ca_3Ga_2N_4$.[32] $Eu_3Ga_2P_4$ is the first example of this structure containing a magnetic element. In addition, the physical properties of a compound with this structure type are examined for the first time in the present study. The structure is characterized by a pair of edge-shared GaP_4 tetrahedra, which are connected by other tetrahedra to form a $[Ga_2P_6]$ dimer unit. These $[Ga_2P_6]$ dimers connect to each other by sharing corners to make a two-dimensional layer described by the formula $[Ga_2P_{4/2}P_2]$ parallel to the bc plane. The Ga−P network is schematically shown in Figure 2.

dx.doi.org/10.1021/ic202018r | *Inorg. Chem.* 2012, 51, 2860−2866

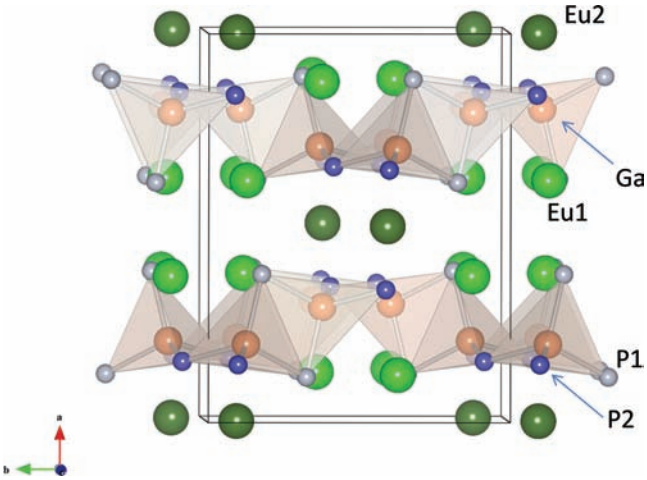

Figure 1. Crystal structure of $Eu_3Ga_2P_4$. Bright-green, dark-green, orange, gray, and blue balls indicate Eu1, Eu2, Ga, P1, and P2, respectively.

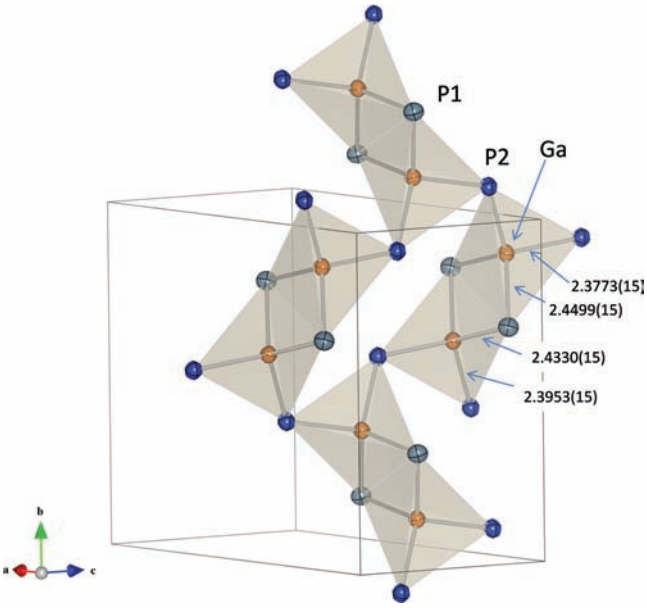

Figure 2. Schematic view of the $[Ga_2P_4]$ network of $Eu_3Ga_2P_4$. Orange, gray, and blue balls indicate Ga, P1, and P2, respectively. Lengths are listed in angstroms. Anisotropic displacement ellipsoids are shown at the 99% probability level.

Such a two-dimensional distribution of the dimer-like unit composed of Ga and P is seen in $EuGa_2P_2$ as well. The bonding network is, however, quite different between the two compounds. In $Eu_3Ga_2P_4$, each Ga atom is tetrahedrally surrounded by four P atoms, with Ga–P distances ranging from 2.3773(15) to 2.4499(15) Å. The shortest Ga–Ga distance within the $[Ga_2P_{4/2}P_2]$ unit is 3.081 Å, much larger than twice that of the Ga covalent radius, 2.5 Å.[33] Thus, bonding within Ga–Ga is considered to be absent; thereby, formation of the dimer and its connection for a two-dimensional network are mediated via Ga–P–Ga bonding in $Eu_3Ga_2P_4$. In contrast, Ga–Ga distances in $EuGa_2P_2$ are 2.404–2.492 Å, very close to or slightly shorter than twice that of the Ga covalent radius, suggesting the existence of Ga–Ga bonding. Thus, each Ga is tetrahedrally coordinated by three P and one Ga atoms. This mixed bonding forms two-dimensional networks of Ga–P in $EuGa_2P_2$.

In a previous study, the existence of a minor phase was suggested for $EuGa_2P_2$, where half of the Ga–Ga dimers are replaced by Eu, resulting in the chemical composition $Eu_3Ga_2P_4$. In this proposed structure, the remaining $[Ga_2P_4]$ units still have Ga–Ga bonding, and the units connect one-dimensionally to form a ladder along the *b* axis. Clearly, this unique structure is not realized in the present compound and may be precipitated as a metastable phase from the $EuGa_2P_2$ matrix.

The $[Ga_2P_{4/2}P_2]$ unit in $Eu_3Ga_2P_4$ composed of a pair of edge-shared $[GaP_4]$ tetrahedra is similar to the $[In_2P_{4/2}P_2]$ unit seen in $Eu_3In_2P_4$.[10] The latter compound has an orthorhombic unit cell and space group *Pnnm* and is isotypic with $Sr_3In_2P_4$ and $Ca_3In_2As_4$.[25] In this structure, an In atom is tetrahedrally coordinated by four P atoms, and two InP_4 tetrahedra are edge-shared to form a $[In_2P_{4/2}P_2]$ dimer unit. The units form a one-dimensional ladder structure by corner-sharing.

There are two Eu sites, Eu1 and Eu2, in $Eu_3Ga_2P_4$. Eu1 is located on both sides of the $[Ga_2P_4]$ layer, as can be seen in Figure 1. Eu2 is placed between the two $[Ga_2P_4]$ layers. Each Eu atom is surrounded by six P atoms with a distorted octahedral environment. The Eu local coordination by P is schematically shown in Figure 3. The bond lengths between Eu1 and P atoms differ from 2.9519(14) to 3.3929(14) Å. On the other hand, the distances between the Eu2 and P atoms fall within a narrower range from 2.9372(13) to 3.1114(14) Å. This would be because the Eu2 site is in the middle of two $[Ga_2P_4]$ layers and is more symmetric (4e) than Eu1 with an 8f position. All of these bond lengths are slightly larger than the sum of the covalent radii of Eu and P, 2.79 Å, but most of them are smaller than the sum of the ionic radii of Eu^{2+} and P^{3-}, 3.34 Å.[33] Therefore, weak covalent bonding between the nearest Eu and P sites may be significant.

$Eu_3Ga_2P_4$ shows a semiconducting behavior, as will be shown later. This is consistent with the charge balance of the compound when each Eu atom provides two electrons to compensate for the negative charge of the $[Ga_2P_2P_{4/2}]^{6-}$ polyanion. Thus, $Eu_3Ga_2P_4$ is described by the Zintl concept, similarly to $Ca_3Ga_2N_4$.

Magnetic Properties. Figure 4 shows the temperature dependence of the magnetic susceptibility, χ, for a single crystal of $Eu_3Ga_2P_4$ measured at a constant magnetic field of H = 100 G. The inset of Figure 4 shows the temperature dependence of the inverse susceptibility $(1/\chi)$. A linear temperature dependence of $1/\chi$ is seen from 300 K to about 20 K. The magnetic susceptibility is, hence, analyzed by the Curie–Weiss law:

$$\chi = \frac{C}{T - \theta}$$

where C and θ are Curie constant and Weiss temperature, respectively. Here, the temperature-independent term to χ has been neglected. The data are fit with this function, yielding C = 7.316(60) emu K/Eu-mol and θ = 24(1) K. The Curie constant is expressed as $C = N_A\mu_{eff}^2/3k_B$, where N_A is Avogadro's number, μ_{eff} an effective magnetic moment, and k_B Boltzmann's constant. The obtained value of C gives μ_{eff} = 7.65(3) μ_B. This is close to the value of 7.937 μ_B, expected for an Eu^{2+} ion with total angular momentum $J = {}^7/_2$ and the Landé g factor = 2.

The positive value of θ indicates that the magnetic interaction between Eu^{2+} ions is ferromagnetic. Magnetic susceptibility, χ, indeed increases rapidly below 20 K and

dx.doi.org/10.1021/ic202018r | Inorg. Chem. 2012, 51, 2860–2866

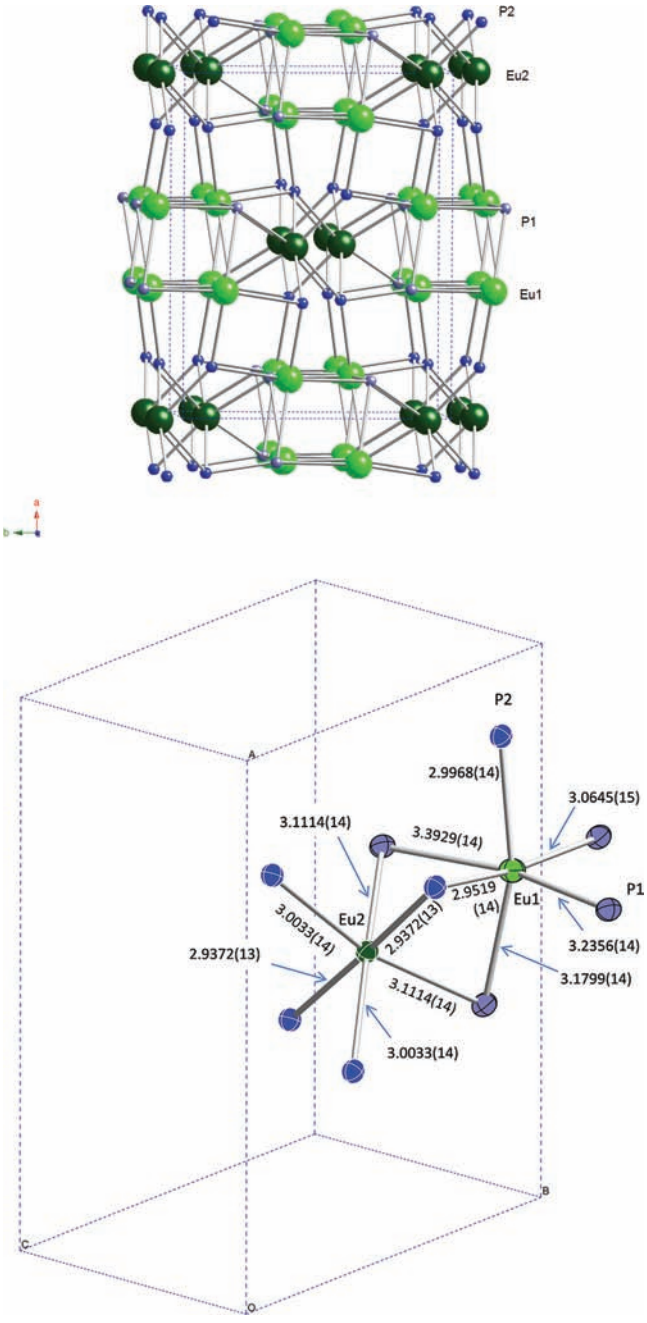

Figure 3. (Top) View of the three-dimensional networks of EuP_6 octahedra in $Eu_3Ga_2P_4$. Ga atoms are not shown in this view. (Bottom) Local environments of Eu1 and Eu2 atoms. Lengths are listed in angstroms. The anisotropic displacement ellipsoids are shown at the 99% probability level.

saturates at lower temperatures, pointing to a ferromagnetic transition. The Curie temperature, T_C, is estimated to be 15 K, from the temperature where the temperature derivative of magnetic susceptibility, $d\chi/dT$, changes its sign. Below this temperature, χ shows magnetic anisotropy. χ for $H\|b$ increases with decreasing T, while χ for $H\perp b$ is independent of the temperature, suggesting that the magnetic easy axis is parallel to the b direction. The value of T_C = 15 K is very close to the magnetic transition temperatures in other Eu-containing Zintl compounds: e.g., 14 K for Eu_3InP_3 and 15 K for $Eu_{14}InSb_{11}$, etc.[4,9] Below T_C, $\chi-T$ data split between zero-field-cooled (ZFC) and field-cooled (FC) measurements. It is unusual that

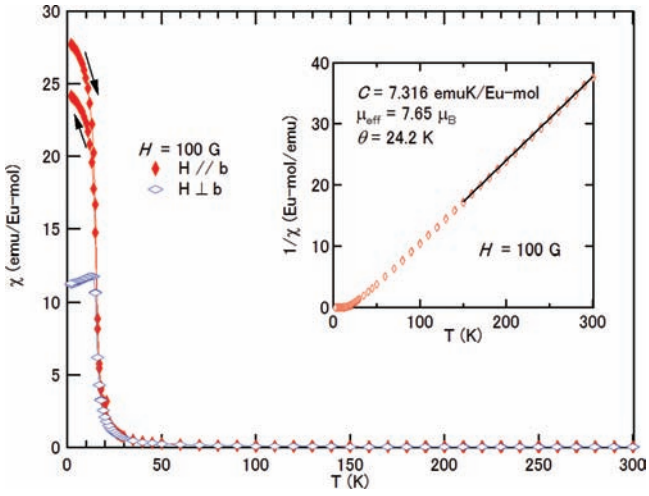

Figure 4. Magnetic susceptibility, χ, of $Eu_3Ga_2P_4$ measured for a single crystal at a constant field of H = 100 G. Inset: inverse of susceptibility, $1/\chi$, measured at H = 100 G with the b axis parallel to H.

ZFC data are greater than FC data, as seen in Figure 4. Similar behavior has been reported in $LaVO_3$ and YVO_3,[34,35] where a large hysteresis is seen in ZFC and FC magnetizations, with ZFC magnetization larger than that of FC. The anomalous hysteresis has been explained via the competition of a single-ion anisotropy and antisymmetric interaction in a canted-antiferromagnetic system. It is not clear whether the same mechanism can be applied to our case. It is also possible that the crystal orientation may have been slightly tilted from the easy direction during the heating cycle.

In Figure 5, the field dependence of magnetization measured at T = 2 K is shown. For field parallel to the b axis,

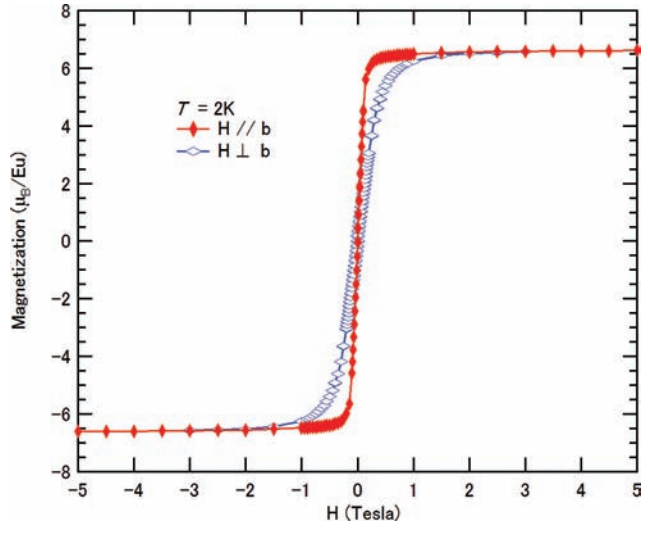

Figure 5. Field dependence of magnetization (M) for $Eu_3Ga_2P_4$ measured at T = 2 K.

magnetization increases rapidly and saturates to 6.6 μ_B. This value is close to the expected magnetic moment for Eu^{2+} ions, $gJ_z\mu_B = 7\ \mu_B$. When the field is applied perpendicularly to the b axis, magnetization saturates to the same value but increases gradually compared to the case of $H\|b$. This indicates that the magnetic easy direction of $Eu_3Ga_2P_4$ is parallel to the b axis and is consistent with the anisotropic behavior in $\chi-T$.

dx.doi.org/10.1021/ic202018r | Inorg. Chem. 2012, 51, 2860–2866

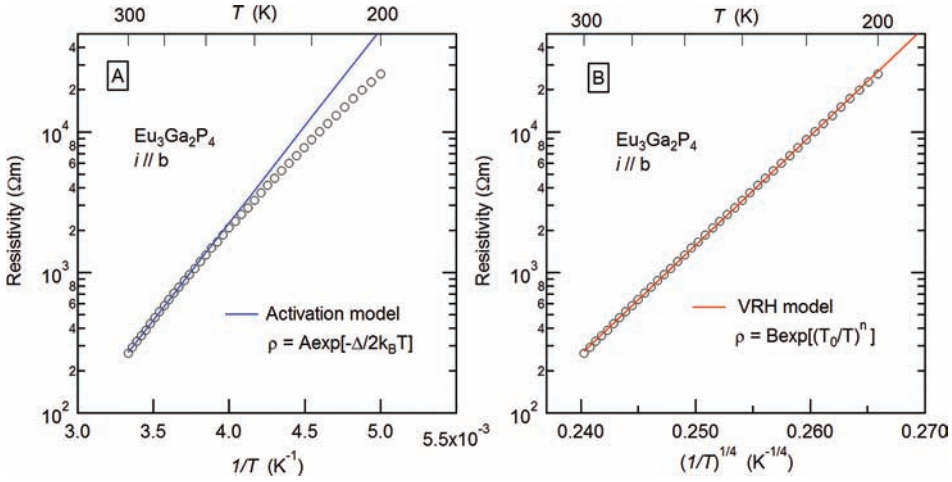

Figure 6. Temperature dependence of the electrical resistivity measured with a current parallel to the b axis. (A) Resistivity as a function of $1/T$. The solid line represents a fit to the data near room temperature using an activation model, $\rho = A\exp[\Delta/2k_BT]$, with $\Delta/k_B = 6412(31)$ K. (B) Resistivity plotted as a function of $(1/T)^{1/4}$. The solid line represents a fit using the VRH model, $\rho = B\exp[(T_0/T)^n]$ with $T_0/10^6 = 610(7)$ K and $n = 0.257(31)$.

Electrical Resistivity. Figure 6 shows the temperature dependence of the electrical resistivity, measured with a current parallel to the b axis. Resistivity at room temperature has a large value close to the kilometer ohm range and increases exponentially with decreasing temperature. The data are analyzed by an activation model, $\rho = A\exp[\Delta/2k_BT]$. However, as is shown in Figure 6A, where ln ρ is plotted as a function of $1/T$, the activation model is not applicable for a wide temperature range because the linearity between ln ρ and $1/T$ is only valid between 280 and 300 K. The fitting yields $\Delta = 8.769 \times 10^{-20}$ J, which corresponds to 6412(31) K or 0.552(2) eV. The value of the energy gap is close to that of $Eu_3In_2P_4$ with an orthorhombic unit cell ($Pnnm$), 0.452 eV.[10] The value of Δ is not reliable because the applicable T range for the activation model is too narrow. This rather implies that the simple activation model is not appropriate for the present case. Instead, we examined the analysis using the variable-range-hopping (VRH) model, $\rho = B\exp[(T_0/T)^n]$, where B, T_0, and n are parameters.[36−38] Here, the exponent n is described as $n = 1/(d+1)$, where d represents the dimension of the conduction mechanism. Fitting with this equation for the whole temperature range yielded $B = 1.98 \times 10^{-16}$ Ω m, $T_0/10^6 = 610(7)$ K, and $n = 0.257(31)$. The fitted curve agrees well with the data, as is seen in Figure 6B. Furthermore, the exponent $n = 0.257$ is very close to $^1/_4$, suggesting that the conduction is mostly three-dimensional ($d = 3$). This is in contrast with the two-dimensional Ga−P networks shown in Figures 1 and 2. This suggests that Eu−P bonding is involved in the carrier conduction in $Eu_3Ga_2P_4$ because P−Eu−P bonding bridges two Ga_2P_4 layers to form a three-dimensional network, as is shown in Figure 3.

In Figure 7, the temperature dependence of the electrical resistance measured at $H = 2$ T is shown. A two-probe method was applied for this measurement in order to measure to lower temperatures; thereby, absolute values of the resistivity are not known. Plotted in the inset of Figure 6 is the MR ratio, $[R(H) - R(0)]/R(0) \times 100$ at $H = 2$ T, as a function of the temperature. The MR ratio becomes pronounced with decreasing temperature and reaches −30% at 100 K.

The MR effect has also been investigated for the Zintl compound $Eu_3In_2P_4$. It shows a negative MR ratio up to −30%

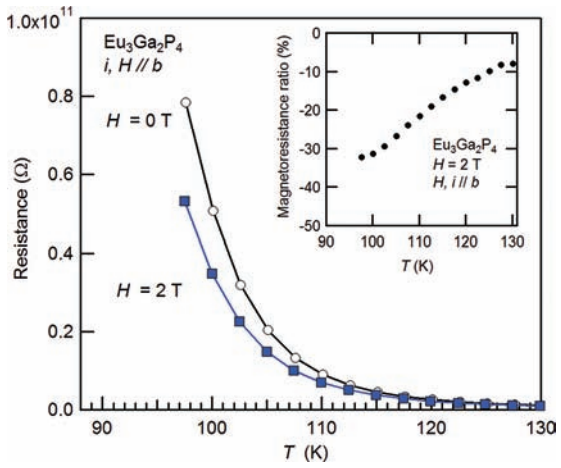

Figure 7. MR of $Eu_3Ga_2P_4$ with a current parallel to the b axis. Magnetic field $H = 2$ T is applied parallel to the current. The inset shows the MR ratio, $[R(H) - R(0)]/R(0) \times 100$.

at 2 K with fields of 5 T.[10] The MR effect of $Eu_3In_2P_4$ is pronounced below its ferromagnetic ordering temperature, $T_C = 14.5$ K, while the MR appears to be negligible for temperatures higher than 30 K. A large MR has also been observed in $EuGa_2P_2$ and $EuIn_2P_2$, for which the maximum values of the MR ratio at a field of 5 T reach −80% and −300%, respectively.[11,13] This colossal decrease in the resistivity occurs at temperatures close to their ferromagnetic transition temperature, $T_C = 24$ K. Again, magnetic fields up to 5 T do not appear to cause a significant decrease in the resistivity for temperatures around 100 K. The MR ratio of −30% for $Eu_3Ga_2P_4$ at $H = 2$ T is therefore anomalously high considering the recorded temperature of 100 K, which is over 6 times higher than its $T_C = 15$ K. This indicates that the carriers in this compound, either electrons or holes, are very strongly coupled to the Eu^{2+} magnetic moment. We also mention that a field-induced phase transition at 2 T is unlikely because the $\chi-T$ data measured at 2 T agree well with those measured at 100 G (Supporting Information) above 50 K.

Here it should be noted that the electrical resistivity has been well described by a three-dimensional VRH model, as is shown

dx.doi.org/10.1021/ic202018r | Inorg. Chem. 2012, 51, 2860−2866

in Figure 6B. This indicates that the Eu−P bond path is involved in carrier conduction. Moreover, hopping conductivity generally occurs when the mean free path of carriers is so short that the wavenumber k is not a good quantum number and carriers are nearly localized around the impurity centers.[39] Here, the Eu−P bonds in $Eu_3Ga_2P_4$ have nine different bonds lengths, as is shown in Figure 3. This complicated coordination circumstance may act as a semirandom potential when carriers find pathways through the Eu−P bonds, giving rise to the VRH conductivity. On the other hand, it is also possible that the VRH behavior is due to defects and disorders in the crystal. In any case, the observed three-dimensional VRH conductivity means that the carrier path through the Eu−P bond is important and, hence, the large MR can be the result of strong interaction between the carrier and the Eu^{2+} magnetic moment at the Eu sites. Strong coupling between carriers and magnetic moments have been discussed for EuB_6, EuO, and Eu monochalcogenides, where the MR effect is significant even above T_C,[15−19] and magnetic polarons are proposed.[18,19] The present compound is, hence, a very intriguing system to study the coupling mechanisms between carriers and magnetic moments that can produce the giant MR effect.

One can expect that the MR effect in $Eu_3Ga_2P_4$ is further enhanced for lower temperatures, especially near T_C, although the present measurements at lower temperatures were not possible because of the high resistance. Slightly tuning the carriers through chemical substitutions would reduce the resistivity and might allow for further characterization of the electronic transport at low temperatures. In addition, band calculation would be helpful to reveal the origin of the strong coupling between the charge carrier and the Eu^{2+} magnetic moment.

CONCLUSION

A new Zintl compound, $Eu_3Ga_2P_4$, has been characterized using single crystals grown by a Ga-flux technique. Single-crystal X-ray diffraction taken at 90 K reveals that $Eu_3Ga_2P_4$ is isostructural to $Ca_3Al_2As_4$ with a monoclinic unit cell, space group $C2/c$ (No. 15), and lattice parameters a = 13.0245(12) Å, b = 10.1167(10) Å, c = 6.5580(6) Å, and β = 90.2430(0)°. The Ga atoms are tetrahedrally surrounded by four P atoms. Pairs of tetrahedra are edge-shared to form dimer-like units, which connect to each other by corner-sharing and stack along the bc direction two-dimensionally. Magnetic susceptibility shows a Curie−Weiss behavior with an effective magnetic moment consistent with the Eu^{2+} ion. Thus, $Eu_3Ga_2P_4$ can be written as $[Eu^{2+}]_3[Ga_2P_4]^{6-}$ and is classified as a charge-balanced Zintl compound.

A ferromagnetic transition is observed below 15 K, with the magnetic easy axis parallel to the b direction. The saturated magnetic moment is 6.6 μ_B per Eu, close to that expected for a Eu^{2+} ion, 7 μ_B. Electrical resistivity shows semiconducting behavior. The opening of an energy gap is consistent with the Zintl concept. Fitting the resistivity using an activation model yielded an energy gap of 0.552(2) eV. The fitting was, however, only applicable in a very narrow temperature range between 280 and 300 K. Instead, the VRH model $\rho = B \exp[(T_0/T)^n]$ gave a satisfactory agreement with the data for the whole temperature range measured, with the exponent n = 0.257(31). This value of n is very close to that expected for the three-dimensional conduction, $n = {}^1/_4$. Because the crystal structure of $Eu_3Ga_2P_4$ is composed of the Ga_2P_4 layer and the Eu atoms inserted between the Ga_2P_4 layers, three-dimensional conductivity suggests that P−Eu−P bonding is involved in carrier conduction. This conducting path may lead to the on-site interaction of carriers with Eu^{2+} local moments. Indeed, a pronounced MR is observed. The MR ratio at H = 2 T reaches −30% for T = 100 K, which is unusually large compared to the MR effect observed at this temperature for Eu-containing Zintl compounds. The MR is expected to be further enhanced at lower temperatures. Tuning the carrier concentration through chemical substitutions may provide further insight into the electronic and magnetic property interdependence.

ASSOCIATED CONTENT

Supporting Information

Crystallographic data in CIF format and temperature dependence of magnetization measured at H = 2 T. This material is available free of charge via the Internet at http://pubs.acs.org.

AUTHOR INFORMATION

Corresponding Author

*E-mail: tsujii.naohito@nims.go.jp.

Notes

The authors declare no competing financial interest.

ACKNOWLEDGMENTS

This research was funded by the NSF (Grants DMR-0600742 and DMR-1100313). We thank Jim Fettinger for assistance with crystallography. N.T. acknowledges financial support by the Japan Society for the Promotion of Science.

REFERENCES

(1) Kauzlarich, S. M. *Chemistry, Structure, and Bonding of Zintl Phases and Ions*; VCH Publishers: New York, 1996.
(2) Kauzlarich, S. M.; Brown, S. R.; Snyder, G. J. *Dalton Trans.* **2007**, 2099.
(3) Toberer, E. S.; May, A. F.; Snyder, G. J. *Chem. Mater.* **2010**, *22*, 624.
(4) Chan, J. Y.; Kauzlarich, S. M.; Klavins, P.; Shelton, R. N.; Webb, D. J. *Chem. Mater.* **1997**, *9*, 3132.
(5) Ramirez, A. P. *J. Phys.: Condens. Matter* **1997**, *9*, 8171.
(6) Tokura, Y. *Rep. Prog. Phys.* **2006**, *69*, 797.
(7) Brown, S. R.; Kauzlarich, S. M.; Gascoin, F.; Snyder, S. J. *Chem. Mater.* **2006**, *18*, 1873.
(8) Moreschini, L.; Dallera, C.; Joyce, J. J.; Sarrao, J. L.; Bauer, E. D.; Fritsch, V.; Bobev, S.; Carpene, E.; Huotari, S.; Vankó, G.; Monaco, G.; Lacovig, P.; Panaccione, G.; Fondacaro, A.; Paolicelli, G.; Torelli, P.; Grioni, M. *Phys. Rev. B* **2007**, *75*, 035113.
(9) Jiang, J.; Payne, A. C.; Olmstead, M. M.; Lee, H. Oh.; Klavins, P.; Fisk, Z.; Kauzlarich, S. M.; Hermann, R. P.; Grandjean, F.; Long, G. J. *Inorg. Chem.* **2005**, *44*, 2189.
(10) Jiang, J.; Olmstead, M. M.; Kauzlarich, S. M.; Lee, H. Oh.; Klavins, P.; Fisk, Z. *Inorg. Chem.* **2005**, *44*, 5322.
(11) Jiang, J.; Kauzlarich, S. M. *Chem. Mater.* **2006**, *18*, 435.
(12) Goforth, A. M.; Klavins, P.; Fettinger, J. C.; Kauzlarich, S. M. *Inorg. Chem.* **2008**, *47*, 11048.
(13) Goforth, A. M.; Hope, H.; Condron, C. L.; Kauzlarich, S. M.; Jensen, N.; Klavins, P.; MaQuilon, S.; Fisk, Z. *Chem. Mater.* **2009**, *21*, 4480.
(14) Pfuner, F.; Degiorgi, L.; Ott, H.-R.; Bianchi, A.; Fisk, Z. *Phys. Rev. B* **2008**, *77*, 024417.
(15) Guy, C. N.; von Molnar, S.; Etourneau, J.; Fisk, Z. *Solid State Commun.* **1980**, *33*, 1055.
(16) Süllow, S.; Prasad, I.; Bogdanovich, S.; Aronson, M. C.; Sarrao, J. L.; Fisk, Z. *J. Appl. Phys.* **2000**, *87*, 5591.
(17) Oliver, M. R.; Dimmock, J. O.; McWhorter, A. L.; Reed, T. B. *Phys. Rev. B* **1972**, *5*, 1078.

(18) Kasuya, T.; Yanase, A. *Rev. Mod. Phys.* **1968**, *40*, 684.
(19) Mauger, A.; Godart, C. *Phys. Rep.* **1986**, *141*, 51.
(20) Rauscher, J. F.; Condron, C. L.; Beault, T.; Kauzlarich, S. M.; Jensen, N.; Klavins, P.; MaQuilon, S.; Fisk, Z.; Olmstead, M. M. *Acta Crystallogr.* **2009**, *C65*, i69.
(21) Mathieu, J.; Achey, R.; Park, J.-H.; Purcell, K. M.; Tozer, S. W.; Latturner, S. E. *Chem. Mater.* **2008**, *20*, 5675.
(22) He, H.; Stearrett, R.; Nowak, E. R.; Bobev, S. *Inorg. Chem.* **2010**, *49*, 7935.
(23) Singh, N.; Schwingenschlögl, U. *Chem. Phys. Lett.* **2011**, *508*, 29.
(24) Cordier, G.; Czech, E.; Jakowski, M.; Schäfer, H. *Rev. Chim. Mineral.* **1981**, *18*, 9.
(25) Cordier, G.; Schäfer, H.; Stelter, M. *Z. Naturforsch.* **1986**, *41b*, 1416.
(26) Canfield, P. C.; Fisk, Z. *Philos. Mag. B* **1992**, *65*, 1117.
(27) Kanatzidis, M. G.; Pöttgen, R.; Jeitschko, W. *Angew. Chem., Int. Ed.* **2005**, *44*, 6996.
(28) *SMART, SAINT+, and SADABS*; Bruker AXS: Madison, WI, 1998.
(29) Sheldrick, G. M. *SHELXTL*, 6.10 ed.; Bruker Analytical X-ray Instruments, Inc.: Madison, WI, 1997.
(30) Somer, M.; Carrillo-Cabrera, W.; Peters, K.; von Schnering, H. G. *Z. Kristallogr. - New Chem. Struct.* **1998**, *213*, 4.
(31) Somer, M.; Carrillo-Cabrera, W.; Peters, K.; von Schnering, H. G. *Z. Kristallogr. - New Chem. Struct.* **1998**, *213*, 230.
(32) Clarke, S. J.; DiSalvo, F. J. *Inorg. Chem.* **1997**, *36*, 1143.
(33) Emsley, J., Ed. *Elements*; Oxford University Press Inc.: New York, 1989.
(34) Mahajan, A. V.; Johnston, D. C.; Torgeson, D. R.; Borsa, F. *Phys. Rev. B* **1992**, *46*, 10966.
(35) Ren, Y.; Palstra, T. T. M.; Khomskii, D. I.; Nugroho, A. A.; Menovsky, A. A.; Sawatsky, G. A. *Phys. Rev. B* **2000**, *62*, 6577.
(36) Mott, N. F. *Philos. Mag.* **1969**, *19*, 835.
(37) Mott, N. F. *Adv. Phys.* **1972**, *21*, 785.
(38) Brenig, W.; Döhler, G. H.; Heyszenau, H. *Philos. Mag.* **1973**, *27*, 1093.
(39) Ziman, J. M. *Principles of the Theory of Solids*; Cambridge University Press: New York, 1972.